https://doi.org/10.5194/essd-2020-345
Preprint. Discussion started: 29 December 2020
© Author(s) 2020. CC BY 4.0 License.

Open Access Earth System Science Data Discussions

Long time series of daily evapotranspiration in China based on the SEBAL model and multisource images and validation

Minghan Cheng[1,2,3], Xiyun Jiao[1,3*], Binbin Li[4], Xun Yu[2], Mingchao Shao[2], Xiuliang Jin[2*]

[1]Hohai University, College of Agricultural Science and Engineering, Nanjing, Jiangsu Province, 210048, PR China
[2]Institute of Crop Sciences, Chinese Academy of Agricultural Sciences/Key Laboratory of Crop Physiology and Ecology, Ministry of Agriculture, Beijing 100081, PR China
[3]State Key Laboratory of Hydrology-Water Resources and Hydraulic Engineering, Nanjing, Jiangsu Province, 210048, PR China
[4]Monitoring Center of Soil and Water Conservation, Ministry of Water Resources of the People's Republic of China, Beijing, 100053, PR China

Correspondence to: Xiyun Jiao (xyjiao@hhu.edu.cn) and Xiuliang Jin (jinxiuliang@caas.cn)

Abstract. Satellite observations of evapotranspiration (ET) have been widely used for water resources management in China. An accurate ET product with a high spatiotemporal resolution is required for research on drought stress and water resources management. However, such a product is currently lacking. Moreover, the performances of different ET estimation algorithms for China have not been clearly studied, especially under different environmental conditions. Therefore, the aims of this study were as follows: (1) to use multisource images to generate a long time series (2001-2018) daily ET product with a spatial resolution of 1 km × 1 km based on the Surface Energy Balance Algorithm for Land (SEBAL); (2) to comprehensively evaluate the performance of the SEBAL ET in China using flux observational data and hydrological observational data; (3) to compare the performance of the SEBAL ET with the MOD16 ET product at the point-scale and basin-scale under different environmental conditions in China. At the point-scale, both the models performed best in the conditions of forest cover, subtropical zones, hilly terrain, or summer, respectively, and SEBAL performed better in most conditions. In general, the accuracy of the SEBAL ET (rRMSE = 44.91%) was slightly higher than that of the MOD16 ET (rRMSE = 48.72%). In the basin-scale validation, both the models performed better than in the point-scale validation, with SEBAL obtaining superior results (rRMSE = 19.15%) to MOD16 (rRMSE = 33.62%). Additionally, both the models showed a negative bias, with the bias of the MOD16 ET being higher than that of the SEBAL ET. In the daily-scale validation, the SEBAL ET product showed an RMSE of 0.92 mm/d and an r-value of 0.79. In general, the SEBAL ET product can be used for the qualitative analysis and most quantitative analysis of regional ET. SEBAL ET product is freely available at https://doi.org/10.5281/zenodo.4218413 (Cheng, 2020). The results of this study can provide a reference for the application of remotely sensed ET products and the improvement of satellite ET observation algorithms.

Keyword: evapotranspiration; SEBAL; MOD16; accuracy validation; multiscale

https://doi.org/10.5194/essd-2020-345
Preprint. Discussion started: 29 December 2020
© Author(s) 2020. CC BY 4.0 License.

1. Introduction

Evapotranspiration (ET) is the process of transferring surface water to the atmosphere, including soil evaporation and vegetation transpiration (Wang and Dickinson, 2012). This process is a key node linking surface water and energy balance. In the process of water balance, ET represents the consumption of surface water resources, and in the process of energy balance, the energy consumed by ET is called the latent heat flux (λET, W/m^2, where λ is the latent heat vaporization), which is an important energy component (Helbig et al., 2020; Zhao et al., 2019). Approximately 60% of global precipitation ultimately returns to the atmosphere through evapotranspiration (Wang and Dickinson, 2012). Therefore, accurately quantifying the ET of different land cover types is necessary to better understand changes in regional water resources. However, traditional methods for the estimation of ET based on point-scale or small-area-scale analysis cannot meet the requirement of global climate change research and regional water resource management (Li et al., 2018). Since the United States successfully launched the first meteorological satellite in the 1960s, hydrological remote sensing (RS) applications have developed rapidly and have led to huge breakthroughs (Karimi and Bastiaanssen, 2015). Remote sensing technology with a high spatiotemporal continuity provides an effective means for regional ET estimation.

Satellite remote sensing provides a reliable direct estimation of ground parameters; however, it cannot measure ET directly (Wang and Dickinson, 2012). Therefore, several RS-based algorithms for the estimation of ET have been proposed and reviewed (Pôças et al., 2020; Senay et al., 2020; Wang and Dickinson, 2012). These models can be divided into two types according to their mechanism: those based on surface energy balance (SEB) and those based on semi-empirical formulas (SEFs). SEB-based models can be further divided into one-source models and two-source models (Wang and Dickinson, 2012). One-source models do not distinguish vegetation from bare soil and regard the land surface as a system that exchanges energy and water with the atmosphere. Examples of one-source models include the Surface Energy Balance Index (S-SEBI) (Roerink et al., 2000), the Surface Energy Balance System (SEBS) (Su, 1999), and the Surface Energy Balance Algorithm for Land (SEBAL) (Bastiaanssen et al., 1998a; Bastiaanssen et al., 1998b). These models have a theoretical basis, a simple principle, strong portability, and have been widely used (Bastiaanssen and Steduto, 2017; Elnmer et al., 2019; Huang et al., 2015; Wagle et al., 2019). Two-source models distinguish the surface water and energy exchange between vegetation and bare soil and calculate fractional canopy coverage (*Fc*) using an empirical formula and a vegetation index obtained from remote sensing data to divide the land surface into vegetation and bare soil in each single pixel. Examples of two-source models include the Two-source Energy Balance (TSEB) (Kustas et al., 2003), Two-source Trapezoid Model for Evapotranspiration (TTME) (Long and Singh, 2012), and Hybrid Dual-source Scheme and Trapezoid Framework-based Evapotranspiration Model (HTEM) (Yang and Shang, 2013). Compared to one-source models, two-source models have a superior theoretical mechanism. SEF-based models using traditional semi-empirical formulas calculate λET and are simpler than SEB-based models. Examples of SEF-based models include the Surface Temperature and Vegetation Index (T_s-VI) space model (Carlson, 2007) and the Global Land Evaporation Amsterdam Model (GLEAM) based on the Priestley–Taylor (P-T) equation (Miralles et al., 2011).

https://doi.org/10.5194/essd-2020-345
Preprint. Discussion started: 29 December 2020
© Author(s) 2020. CC BY 4.0 License.

Another well-known SEF-based model is based on the Penman–Monteith (P-M) equation, which has been improved and applied to remote sensing data to estimate regional ET (Mu et al., 2007; Mu et al., 2011).

Since ET plays a critical role in the study of hydrology and ecology, ET products with a high spatiotemporal resolution are required. Therefore, a growing number of ET products have been generated to meet research needs. These include MOD16, which is generated by NASA based on the P-M algorithm and has a spatial resolution of 500 m × 500 m and a temporal resolution of eight days (Mu et al., 2007; Mu et al., 2011). However, a temporal resolution of eight days is not sufficient to conduct research on water resource management. The GLEAM daily ET product with a spatial resolution of 0.25° × 0.25° has been generated by the University of Bristol, UK, based on the P-T equation (Miralles et al., 2010). Additionally, Chen generated long time series daily ET datasets with a spatial resolution of 0.1° × 0.1° based on the SEBS algorithm (Chen et al., 2014; Chen, 2019). However, there are few ET products which simultaneously meet the current research needs in terms of temporal and spatial resolution. Therefore, generating a kilometer-level daily ET product which can minimize the influence of mixed pixels is critical. Moreover, the accuracy of ET derived from satellite imagery is affected by spatiotemporal conditions (Wagle et al., 2017). Several studies have indicated that RS-based methods for modeling ET have errors of 15–50% (Velpuri et al., 2013; Xue et al., 2020). RS-based models have different applicable conditions, and understanding the variation in accuracy between such models is important for their reasonable application. Several models have been validated by various researchers. For example, Wagle et al. (2017) compared five one-source SEB-models for application to high-biomass sorghum in Oklahoma, USA, and showed that each model has a high accuracy. Xue et al. (2020) compared the application of SEBAL and SEBS in different crops in California, USA, and found that SEBAL had a higher accuracy for full cover crops. Ramoelo et al. (2014) validated MOD16 products in the savanna of South Africa. However, few studies have validated the robustness of different models using long time series and at a large spatial scale, and most have focused on the accuracy validation and comparison of SEB-based models; however, there have been few comparative studies between SEB-based and SEF-based models. Furthermore, the performance of different ET estimation algorithms in China has not been clearly discussed, especially under different environmental conditions.

Water resources management is essential for China as it has an unbalanced spatial and temporal distribution of water resources. However, there is no ET product for China with a high spatiotemporal resolution, and the applicability of different RS-based models for the estimation of ET in China is not clear, which hampers the management of ET. In order to improve ET products in China and better understand the performance of RS-based ET estimation models in China, in this paper, we aim to (1) generate a long time series daily ET product with a spatial resolution of 1 km × 1 km based on the SEBAL model and multisource remote sensing images, (2) validate the accuracy of the generated ET product in China based on flux tower observational data and hydrological data, and (3) compare the performance of the generated ET product with MOD16 datasets in China under different environmental conditions.

https://doi.org/10.5194/essd-2020-345
Preprint. Discussion started: 29 December 2020
© Author(s) 2020. CC BY 4.0 License.

Open Access Earth System Science Data Discussions

2. Materials and methods

2.1 Study area

China (3°31′00″–53°33′47″ N, 73°29′59.79″–135°2′30″ E) covers a land area of approximately 9,600,000 km^2, mainly including temperate zones, warm-temperate zones, subtropical zones, tropical zones, and plateau climate zones. China can be divided into nine basin regions based on the distribution of water resources (Zhang et al., 2011): the Southwest Basin (SwB), Continental Basin (CB), Pearl River Basin (PRB), Yangtze River Basin (YRB), Southeast Basin (SeB), Haihe River Basin (HRB), Yellow River Basin (YeRB), Huaihe River Basin (HuRB), and Songhua and Liaohe River Basin (SLRB) (Fig. 1).

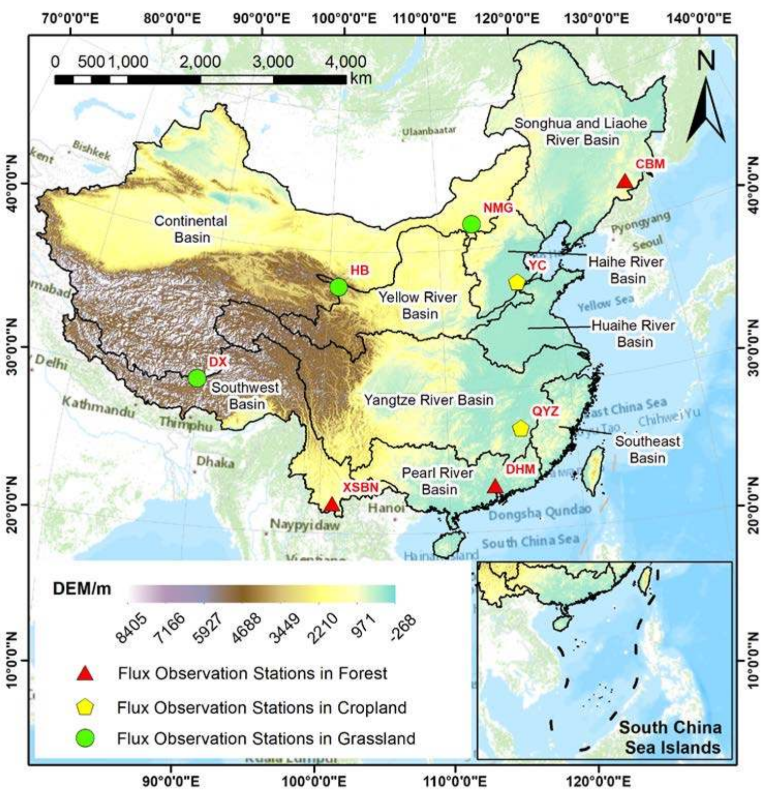

https://doi.org/10.5194/essd-2020-345
Preprint. Discussion started: 29 December 2020
© Author(s) 2020. CC BY 4.0 License.

Open Access Earth System Science Data Discussions

Figure 1. The location of the study area. Note: CBM: Changbai mountain; DHM: Dinghu mountain; DX: Dangxiong; HB: Haibei; NMG: Neimenggu; QYZ: Qianyanzhou; XSBN: Xishuangbanna; YC: Yucheng. (Note: the Chinese boundry was obtained from Institute of Geographic Science and Natural Resources Research, Chinese Academy of Sciences (http://www.resdc.cn/))

2.2 Generation of long time series daily ET product

In this study, a long time series daily ET product was generated based on SEBAL, which is a widely used one-source model (Gobbo et al., 2019; Jaafar and Ahmad, 2020; Mhawej et al., 2020; Rahimzadegan and Janani, 2019). SEBAL has been shown to have a good performance for ET estimation and can be regarded as typical of SEB-based models (Bastiaanssen et al., 1998b; Timmermans et al., 2006; Wagle et al., 2017). The workflow for the calculation of the daily ET using the SEBAL model and multisource satellite images is shown in Fig. 2. The SEBAL model calculates the instantaneous λET of the satellite transit time as a residual based on the surface energy balance equation (Eq. 1) as follows:

$$\lambda ET = R_n - G - H \tag{1}$$

where R_n is the net radiation flux, H is the sensible heat flux, and G is the soil heat flux (the unit of all three parameters is W/m^2). In this paper, MODIS data (MCD43 surface albedo, MOD11 surface temperature, MOD13 NDVI) and meteorological data (air temperature) from the Global Modeling and Assimilation Office (GMAO) were used as input for surface parameterization (R_n, G and H). The equations for R_n are shown in Eqs. 2–5 below:

$$R_n = (1-\alpha)R_s\downarrow + R_l\downarrow - R_l\uparrow \tag{2}$$

where α is the surface albedo obtained from the MCD43 data; $R_s\downarrow$, $R_l\uparrow$, and $R_l\downarrow$ are the downwelling shortwave radiation, downwelling longwave radiation, and upwelling longwave radiation, respectively (the unit of all three parameters is W/m^2). $R_s\downarrow$ can be calculated using the Julian day (used to estimate the astronomical distance between the sun and earth), elevation (used to estimate atmospheric emissivity), and solar zenith angle at the time of satellite transit. $R_l\uparrow$ and $R_l\downarrow$ can be calculated using the surface temperature (MOD11), NDVI (MOD13, used to estimate surface emissivity) and air temperature (GMAO data), and atmospheric emissivity based on the Stefan-Boltzmann law. The equations for $R_s\downarrow$, $R_l\uparrow$, and $R_l\downarrow$ are given in Eqs. 3–5.

$$R_s\downarrow = \frac{G_{sc} \times \cos\theta \times \tau_{sw}}{d_r^{\,2}} \tag{3}$$

$$R_l\uparrow = \varepsilon_a \sigma T_a^4 \tag{4}$$

$$R_l\downarrow = \varepsilon \sigma T_s^4 \tag{5}$$

where G_{sc} is the solar constant (1376 W/m^2); θ is the solar zenith angle; τ_{sw} is the atmospheric transmittance (Eq. 6) (Tasumi, 2000); d_r is the astronomical distance between the sun and earth (Eq. 7) (Bastiaanssen et al., 1998a); ε_a and ε are the atmospheric emissivity (Eq. 8) (Bastiaanssen et al., 1998a) and surface emissivity (obtained from MOD11), respectively; σ is the Stefan-Boltzmann constant (5.67×10^{-8} W/m^{2}K^4); and T_a and T_s are the air temperature (unit: K; obtained from GMAO data) and surface

https://doi.org/10.5194/essd-2020-345
Preprint. Discussion started: 29 December 2020
© Author(s) 2020. CC BY 4.0 License.

temperature (unit: K, obtained from MOD11), respectively.

$$\tau_{sw} = 0.75 \times 2 \times 10^{-5} \times Z \tag{6}$$

$$dr = 1 + 0.0167 \sin(\frac{2\pi(J - 93.5)}{365}) \tag{7}$$

$$\varepsilon_a = 1.08(-\ln \tau_{sw})^{0.265} \tag{8}$$

where Z is the elevation obtained from a DEM (unit: m) and J is the Julian day. G can be calculated by the following empirical equation (Bastiaanssen et al., 1998a):

$$G = R_n \times \frac{T_s - 273.16}{\alpha}(0.0032 \times \frac{\alpha}{c} + 0.0032(\frac{\alpha}{c})^2) \times (1 - 0.978 NDVI^4) \tag{9}$$

where T_s is the surface temperature (unit: K) and c represents the influence of the satellite transit time on G. The value of c is 0.9 for transmission times before 12:00 local time (LT), 1.0 for transmission times between 12:00 and 14:00 LT, and 1.1 for transmission times between 14:00 and 16:00 LT. H can be calculated as follows:

$$H = \frac{\rho_{air} C_p dT}{r_a} \tag{10}$$

where ρ_{air} (unit: kg/m^3) is the air density (Eq. 11) (Smith et al., 1991); C_p (unit: J/(kg×K)) is the specific heat of air at constant pressure; dT (unit: K) is the difference between the aerodynamic surface temperature (T_{z0h}; unit: K) and the reference height temperature (T_a, unit: K); and r_a is the aerodynamic resistance (unit: s/m) (Eq. 12).

$$\rho_{air} = 349.635 \frac{(T_a - 0.0065Z)^{5.26}}{T_a^{6.26}} \tag{11}$$

$$r_a = \frac{\ln(\frac{Z_2}{Z_1})}{kU_f} \tag{12}$$

where k is the von Karman constant (0.41); U_f is the frictional wind speed (unit: m/s) (Eq. 13); and Z_1 and Z_2 are 0.01 and 2, respectively.

$$U_f = \frac{kU_r}{\ln(Z_r / z_{om})} \tag{13}$$

where U_r is the wind speed at height Z_r, which can be calculated from the wind speed monitored by weather stations (U_w, Eq. 14); Z_r is 200 m in this study (Zeng et al., 2008); and z_{0m} is the surface roughness (unit: m, Eq. 15) (Moran and Jackson, 1991).

$$U_r = \frac{U_w \times \ln(67.8 Z_r - 5.42)}{4.87} \tag{14}$$

$$z_{0m} = e^{(5.65 NDVI - 6.32)} \tag{15}$$

However, since it is difficult to calculate dT directly, the model assumes that there is a linear relationship between surface

https://doi.org/10.5194/essd-2020-345
Preprint. Discussion started: 29 December 2020
© Author(s) 2020. CC BY 4.0 License.

temperature (T_s, unit: K) and dT, as shown in Eq. 16:

$$dT = aT_s + b \tag{16}$$

SEBAL solves the values of *a* and *b* by selecting the warmest and coldest spots; it assumes that the warmest spots represent pixels of dry farmland or saline alkali land covered by vegetation with zero λET (H = R_n - G), and the coldest spots represent pixels with sufficient water supply, lush vegetation, and low temperature, with an H of zero (λET = R_n - G). Therefore, *a* and *b* can be expressed as follows:

$$a = \frac{(R_{n\_warmest} - G_{warmest}) r_{a\_warmest}}{C_p \rho_{air\_warmest} (T_{s\_warmest} - T_{s\_coldest})} \tag{17}$$

$$b = -aT_{s\_coldest} \tag{18}$$

Moreover, it should be noted that H and r_a are interrelated variables in the actual calculation; therefore, the Monin–Obkhov Similarity Theory (MOST)-based Monin–Obkhov length (L, unit: m) is introduced for iterative calculation to obtain stable values of H and r_a. The details of MOST are shown in Fig. 3.

The Monin–Obkhov length is a parameter reflecting the turbulent characteristics of the near-surface layer (Eq. 19) (Monin and Obukhov, 1954); $\Psi_m(Z_r)$ is the stability correction function of momentum; and $\Psi_H(Z_1)$ and $\Psi_H(Z_2)$ are the stability correction functions of sensible heat flux (Eqs. 20–28) (Paulson, 1970).

$$L = \frac{\rho_{air} C_p U_f{}^3 T_s}{kgH} \tag{19}$$

where g is the acceleration due to gravity (9.81 m/s^2). While L>0, indicating a stable state, $\Psi_m(Z_r)$, $\Psi_H(Z_1)$, and $\Psi_H(Z_2)$ are calculated as follows:

$$\Psi_m(Z_r) = \frac{-5Z_r}{L} \tag{20}$$

$$\Psi_H(Z_1) = \frac{-5Z_1}{L} \tag{21}$$

$$\Psi_H(Z_2) = \frac{-5Z_2}{L} \tag{22}$$

While L<0, indicating an unstable state, $\Psi_m(Z_r)$, $\Psi_H(Z_1)$, and $\Psi_H(Z_2)$ are calculated as follows:

$$\Psi_m(Z_r) = 2\ln(\frac{1+\zeta_{Z_r}}{2}) + \ln(\frac{1+\zeta_{Z_r}{}^2}{2}) + 2\arctan(\zeta_{Z_r}) + 0.5\pi \tag{23}$$

$$\Psi_H(Z_1) = 2\ln(\frac{1+\zeta_{Z_1}{}^2}{2}) \tag{24}$$

$$\Psi_H(Z_2) = 2\ln(\frac{1+\zeta_{Z_2}{}^2}{2}) \tag{25}$$

https://doi.org/10.5194/essd-2020-345
Preprint. Discussion started: 29 December 2020
© Author(s) 2020. CC BY 4.0 License.

$$\zeta_{z_r} = (1 - \frac{16Z_r}{L})^{0.25} \tag{26}$$

$$\zeta_{z_1} = (1 - \frac{16Z_1}{L})^{0.25} \tag{27}$$

$$\zeta_{z_2} = (1 - \frac{16Z_2}{L})^{0.25} \tag{28}$$

While L=0, indicating a neutral state, $\Psi_m(Z_r) = \Psi_H(Z_1) = \Psi_H(Z_2) = 0$. Then, iterative calculation is carried out to correct H (Eqs. 29–31):

$$U_f^{\ *} = \frac{kU_r}{\ln(Z_r / z_{om}) - \Psi_m(Z_m)} \tag{29}$$

$$r_a^{\ *} = \frac{\ln(\frac{Z_2}{Z_1}) - \Psi_H(Z_1) - \Psi_H(Z_2)}{kU_f^{\ *}} \tag{30}$$

$$H = \frac{\rho_{air} C_p dT}{r_a^{\ *}} \tag{31}$$

Several iterations were carried out until the value of H was stable. Then, Eq. 1 was used to calculate λET. However, it should be noted that all of the estimated energy component was an instantaneous value including latent heat; therefore, the concept of the evaporation fraction (Λ) was used to temporally scale-up from the instantaneous value to the daily ET. The evaporation fraction was defined as the ratio of latent heat to available energy (e.g., R_n-G) (Eq. 32). Several studies have indicated that the evaporation fraction can be regarded as constant throughout the day (Crago, 1996); therefore, the daily ET can be calculated as follows:

$$\Lambda = \frac{\lambda ET}{R_n - G} \tag{32}$$

$$ET_{daily} = \frac{\Lambda(R_{daily} - G_{daily})}{\lambda} \tag{33}$$

where ET_{daily}, R_{daily}, and G_{daily} are the daily evapotranspiration, daily net radiation, and daily soil heat flux, respectively. Finally, the daily ET value was calculated. More details about SEBAL can be found in Bastiaanssen et al. (1998a).

The spatial and temporal resolutions of the MCD43 surface albedo and the MOD11 surface temperature are 1 day and 1 km × 1 km, while those of MOD13 NDVI are 16 days and 500 m × 500 m. In this study, MOD13 was resampled to 1 km × 1 km and processed by smoothing and gap-filling from time series to daily data (Vuolo et al., 2017). The spatial and temporal resolutions of GMAO air temperature are 1 day and 0.25° × 0.25°, respectively. The coarse-resolution GMAO data were non-linearly interpolated to a spatial resolution of 1 km × 1 km based on the four GMAO pixels surrounding a given pixel (Zhao et al., 2005). The spatial and temporal resolutions of wind speed are 1 day and 1 km × 1 km (China Meteorological Data Network, http://data.cma.cn). The final generated

https://doi.org/10.5194/essd-2020-345
Preprint. Discussion started: 29 December 2020
© Author(s) 2020. CC BY 4.0 License.

daily ET product has a spatial resolution of 1 km × 1 km and covers the period 2001 to 2018.

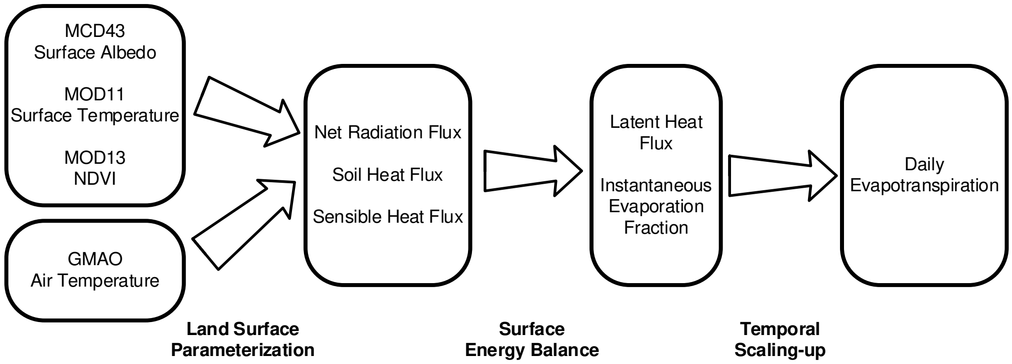

Figure 2. A flowchart of the Surface Energy Balance Algorithm for Land (SEBAL) which was used to convert multisource images to daily evapotranspiration.

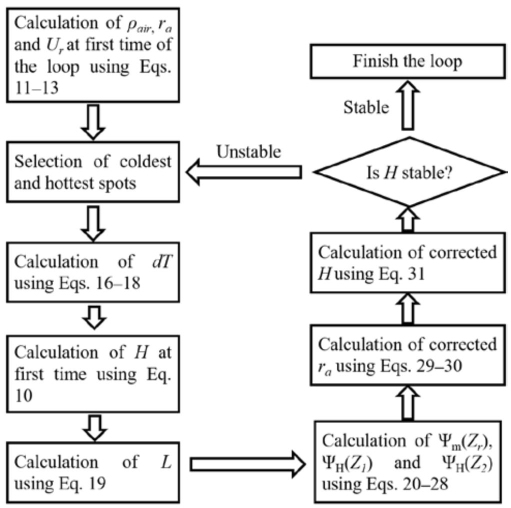

Figure 3. A flowchart of the calculation of sensible heat flux using Monin–Obkhov Similarity Theory (MOST).

2.3 Validation methods

2.3.1 Point-scale validation

The eddy covariance method measures λET using the covariance of vapor and heat fluxes; it is regarded as the most effective method for the estimation of ET and has been widely used (Wang and Dickinson, 2012). In this study, eddy covariance tower-measured daily flux data from eight stations in China (Table 1) obtained in 2003–2010 were used to validate the modeled ET (ET_{SEBAL},

https://doi.org/10.5194/essd-2020-345
Preprint. Discussion started: 29 December 2020
© Author(s) 2020. CC BY 4.0 License.

ET_{MOD}). The latent heat flux (λET) observed at the flux towers was converted into the observed ET (ET_{flux}). The water demand is different under different environmental conditions. Therefore, it is necessary to understand the accuracy performance of ET products for different vegetation types when a single ET product is not comprehensive (Velpuri et al., 2013). In order to better understand the influence of different environmental conditions on the accuracy of the model, the modeled ET were validated for different terrain, climate zones, land cover types, and seasons. Additionally, MOD16 data were resampled to a spatial resolution of 1 km × 1 km and daily ET_{SEBAL} and daily ET_{flux} data were accumulated to eight days to match the MOD16 data. ET_{SEBAL} was validated at the daily scale and 8-day scale, respectively.

Table 1. Details of the eight flux observation stations.

Station	Observation period	Longitude	Latitude	Elevation/m	Climate zone	Land use type
CBM	2003–2010	128.10°E	42.40°N	738 (mountain)	temperate zone	Forest
DHM	2003–2010	112.53°E	23.17°N	319 (hill)	subtropical zone	Forest
DX	2004–2010	91.07°E	30.85°N	5676 (plateau)	plateau climate zone	Grassland
HB	2003–2010	101.29°E	37.62°N	3216 (plateau)	plateau climate zone	Grassland
NMG	2004–2010	116.68°E	43.55°N	1200 (plateau)	temperate zone	Grassland
QYZ	2003–2010	115.06°E	26.74°N	370 (hill)	subtropical zone	Cropland
XSBN	2003–2010	101.20°E	21.96°N	570 (mountain)	tropical zone	Forest
YC	2003–2010	116.60°E	36.95°N	28 (plain)	warm-temperate zone	Cropland

2.3.2 Regional-scale validation

Furthermore, the regional (basin-scale) ET was calculated using the water balance method (Eq. 34) to validate the modeled ET at the regional scale.

$$ET = P - Q - \Delta S \tag{34}$$

where P (unit: mm) is the annual precipitation in the basin; Q (unit: mm) is the annual runoff in the basin, which includes surface runoff and groundwater runoff; ΔS is the change in the groundwater and surface water storage in a year; the change of ΔS at the annual-scale can be ignored. The annual ET was calculated in each primary water resources division in China (the nine basins shown in Fig. 1) from 2001 to 2018; these values of ET are referred to as ET_{WB}.

https://doi.org/10.5194/essd-2020-345
Preprint. Discussion started: 29 December 2020
© Author(s) 2020. CC BY 4.0 License.

2.3.3 Accuracy estimation

The modeled ET values were compared with the observed ET (ET_{flux}, ET_{WB}) to evaluate the performance of ET_{SEBAL} and ET_{MOD}, respectively. The correlation coefficient (r), root-mean-square error (RMSE), relative root-mean-square error (rRMSE), and mean bias error (MBE) were selected to quantify the accuracy of the modeled ET. The equations for these parameters are shown below:

$$r = \frac{\sum_{i=1}^{n}(ET_{Mi} - \overline{ET_M})(ET_{Obi} - \overline{ET_{Ob}})}{\sqrt{\sum_{i=1}^{n}(ET_{Mi} - \overline{ET_M})^2 \sum_{i=1}^{n}(ET_{Obi} - \overline{ET_{Ob}})^2}} \tag{35}$$

$$RMSE = \sqrt{\frac{1}{n}\sum_{i=1}^{n}(ET_{Mi} - ET_{Obi})^2} \tag{36}$$

$$rRMSE = \frac{RMSE}{\overline{ET_{Ob}}} \times 100\% \tag{37}$$

$$MBE = \frac{1}{n}\sum_{i=1}^{n}(ET_{Mi} - ET_{Obi}) \tag{38}$$

where ET_M is the modeled ET (ET_{SEBAL} and ET_{MOD}); ET_{Ob} is the observed ET (ET_{flux} and ET_{WB}); and n is the number of samples. r was calculated to evaluate the linear relationship between the modeled and observed ET; higher r-values mean a higher correlation. RMSE and rRMSE were used to evaluate the absolute bias and relative bias of the modeled ET, respectively: smaller RMSE and rRMSE mean a higher accuracy. rRMSE is a critical indicator to evaluate the accuracy of a model (Jin et al., 2020). The MBE was used to measure whether the result was overestimated (positive values of MBE) or underestimated (negative values of MBE).

2.4 Data sources and tools used

2.4.1 MOD16 data

The MOD16 ET data (ET_{MOD}) were produced using an ET algorithm based on the P-M equation (Eq. 39) (Monteith, 1965) that has been improved (Mu et al., 2007; Mu et al., 2011).

$$\lambda ET = \frac{sA + \rho C_p VPD / r_a}{s + \gamma(1 + r_s / r_a)} \tag{39}$$

where s (unit: Pa/K) is the slope of the temperature-saturated water pressure curve at the current temperature; A (unit: W/m^2) is the available energy; ρ (unit: kg/m^3) is the air density; C_p (unit: J/(kg×K)) is the specific heat of air at constant pressure; VPD (unit: Pa) is the difference in water vapor pressure; γ (unit: Pa/K) is the psychrometric constant; and r_a and r_s (unit: s/m) are the aerodynamic resistance and surface resistance, respectively. The MOD16 ET data are available for regular 500 m grid cells for the entire global vegetated land surface at 8-day composite, and the data do not cover regions corresponding to water, barren land, and buildings (He et al., 2019). In this study, MOD16 data were obtained from the NASA Atmosphere Archive & Distribution System Distributed Active Archive Center (LAADS DAAC, https://ladsweb.modaps.eosdis.nasa.gov).

2.4.2 Auxiliary data

In order to ensure the objectivity of the comparison between the SEBAL and P-M models, MODIS satellite data were selected as the input for SEBAL, including the surface albedo (MCD43), surface temperature (MOD11), and NDVI (MOD13) obtained from LAADS DAAC. Additionally, gridded air temperature data were obtained from the GMAO (https://gmao.gsfc.nasa.gov). Flux-tower observational data were obtained from ChinaFLUX (www.chinaflux.org). Precipitation and runoff data for each basin from 2001 to 2018 were obtained from the Water Resources Bulletin provided by the Ministry of Water Resources of the People's Republic of China (http://www.mwr.gov.cn/).

2.4.3 Tools used

Python (version 3.7; Google Inc., Mountain View, California, USA) and the Geospatial Data Abstraction Library (GDAL; version 3.1.1; Google Inc.) were used to construct SEBAL. The ArcGIS software (version 10.4; Esri Inc., Redlands, California, USA) and ENVI software (version 5.3; Esri Inc.) were used to process raster data. Python and the SPSS software (version 21; IBM Inc., Armonk, New York, USA) were used for numerical calculation and analysis.

3. Results

3.1 Validation of daily SEBAL ET at the point-scale using flux tower observations

The validation results for the daily SEBAL ET (ET_{SEBAL}) obtained using flux tower observational data are shown in Fig. 4. Compared to ET_{flux}, ET_{SEBAL} showed a good performance in China; the two data showed a high consistency, with an r-value of 0.79 with 9896 samples. However, the bias of SEBAL was relatively high; the RMSE and rRMSE were 0.92 mm/d and 42.04%, respectively. As shown in the scatter diagrams in Fig. 4, ET_{SEBAL} showed a negative bias at high values and a positive bias at low values. In general, SEBAL underestimated ET in China, with an MBE of –0.15 mm/d. Moreover, the daily ET_{SEBAL} performed similarly for different land use types. The daily ET_{SEBAL} had a bias of 0.95 mm/d (rRMSE = 37.24%) in cropland and 0.89 mm/d (rRMSE = 44.25%) in grassland, and the daily ET_{SEBAL} underestimated in both cropland and grassland, with MBEs of –0.26 mm/d and –0.44 mm/d, respectively. In forest, the daily ET_{SEBAL} had the highest RMSE of 1.02 mm/d (rRMSE = 41.25%) and the lowest r-value of 0.73, and slightly overestimated compared to ET_{flux} (MBE = 0.09 mm/d). These results suggest that, in general, ET_{SEBAL} is relatively reliable for daily-scale applications.

https://doi.org/10.5194/essd-2020-345
Preprint. Discussion started: 29 December 2020
© Author(s) 2020. CC BY 4.0 License.

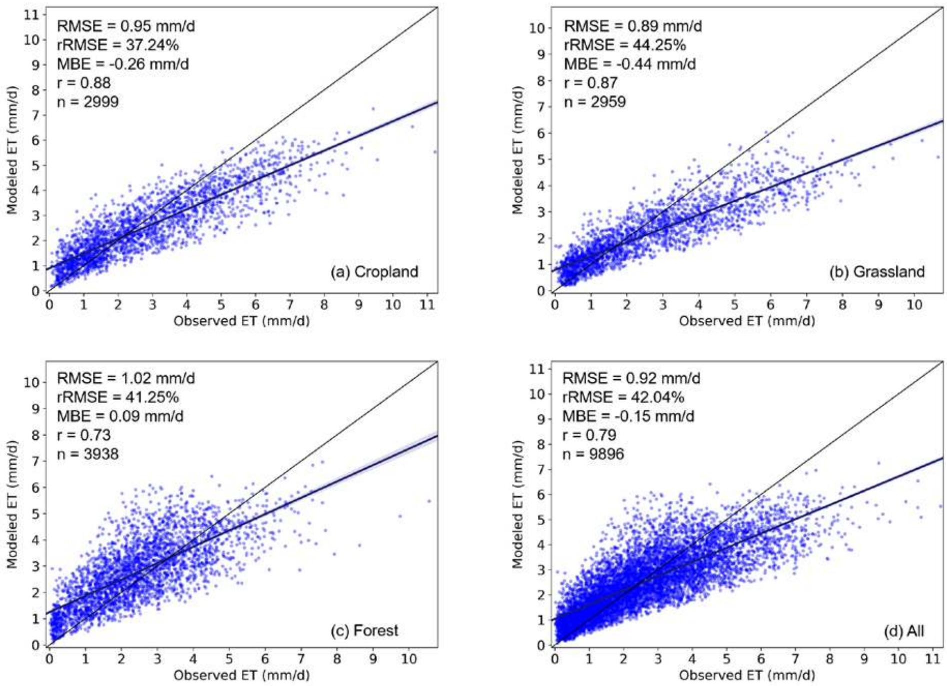

Figure 4. The validation of daily ET estimates using the SEBAL model and multisource images. (a) cropland; (b) grassland; (c) forest; (d) all land cover types.

3.2 Comparison of SEBAL and MOD16 ET under different environmental conditions at the 8-day scale

3.2.1 Performance of the RS-based model for different land cover types

The validation results for different land cover types are shown in Fig. 5. The results indicate that the accuracy of SEBAL and MOD16 both varied with land cover type. The RMSE of SEBAL varied from 6.51 to 8.57 mm/8 d, its rRMSE varied from 38.08 to 52.63%, and its r-value varied from 0.81 to 0.87. The performance of SEBAL was superior for forest (RMSE = 8.54 mm/8 d, rRMSE = 38.08%) compared to other land cover types, and the lowest accuracy was obtained over grassland (RMSE = 6.51 mm/8 d, rRMSE = 52.63%). The results of the MOD16 validation indicate that MOD16 had a better performance for forest (RMSE = 8.88 mm/8 d, rRMSE = 39.29%) than other land cover types, as was observed for SEBAL, and the performance of MOD16 over grassland was also the worst (RMSE = 7.77 mm/8 d, rRMSE = 62.89%). The MBE values for MOD16 varied from 0.42 to 3.44 mm/8 d, which indicated that both the ET models underestimated ET over all land cover types. Overall, the accuracy of SEBAL was higher than that of MOD16.

https://doi.org/10.5194/essd-2020-345
Preprint. Discussion started: 29 December 2020
© Author(s) 2020. CC BY 4.0 License.

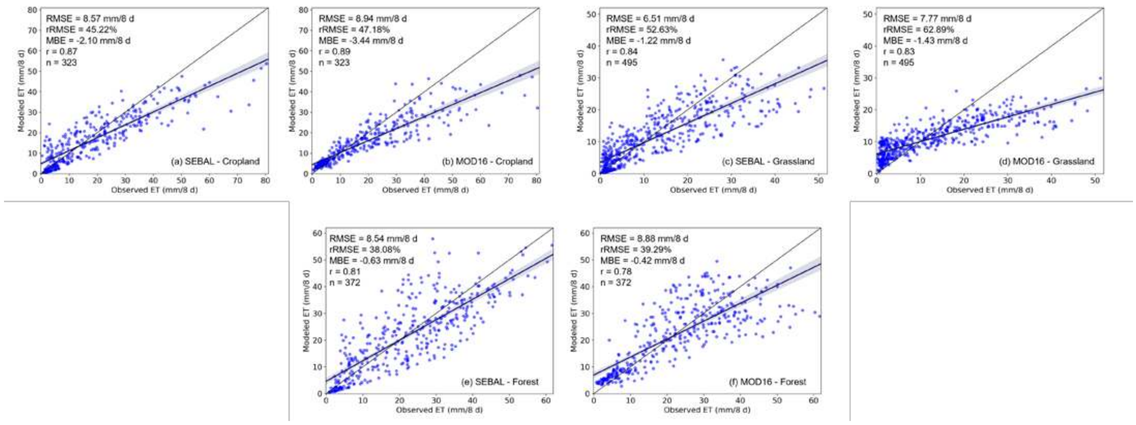

Figure 5. Validations for different land cover types. (a) SEBAL ET for cropland; (b) MOD16 ET for cropland; (c) SEBAL ET for grassland; (d) MOD16 ET for grassland; (e) SEBAL ET for forest; (f) MOD16 ET for forest.

3.2.2 Performance of the RS-based model for different climate zones

The validation results for different climate zones are shown in Fig. 6. The results show that the r-value varied from 0.68 to 0.90 for SEBAL and varied from 0.61 to 0.94 for MOD16. Climate zones were found to influence the accuracy of the RS-based models. In tropical zones, both of the two models showed poor accuracy, with RMSEs of 10.75 and 11.37 mm/8 d for SEBAL and MOD16, respectively, and low r-values of 0.68 and 0.61 for SEBAL and MOD16, respectively. Additionally, both the models overestimated, with MBEs of 7.58 and 8.86 mm/8 d for SEBAL and MOD16, respectively. For subtropical zones, both the models had high precision, with rRMSEs of 32.32% and 36.73% for SEBAL and MOD16, respectively, and both underestimated, with r-values of 0.86 and 0.82 for SEBAL and MOD16, respectively. For warm temperate zones, both SEBAL and MOD16 showed poor accuracy, with rRMSEs of 53.95% and 56.12%, respectively, and both underestimated. For temperate zones, MOD16 overestimated, while SEBAL underestimated, and both models had high r-values, namely 0.90 for SEBAL and 0.94 for MOD16, and low RMSEs of 5.72 mm/8 d for SEBAL and 4.61 mm/8 d for MOD16. In general, MOD16 performed better than SEBAL for temperate zones. For alpine zones with low temperature, both the models still underestimated, however, SEBAL performed better than MOD16: the RMSE was 7.53 and 9.20 mm/8 d and the r-value was 0.79 and 0.77 for SEBAL and MOD16, respectively.

https://doi.org/10.5194/essd-2020-345
Preprint. Discussion started: 29 December 2020
© Author(s) 2020. CC BY 4.0 License.

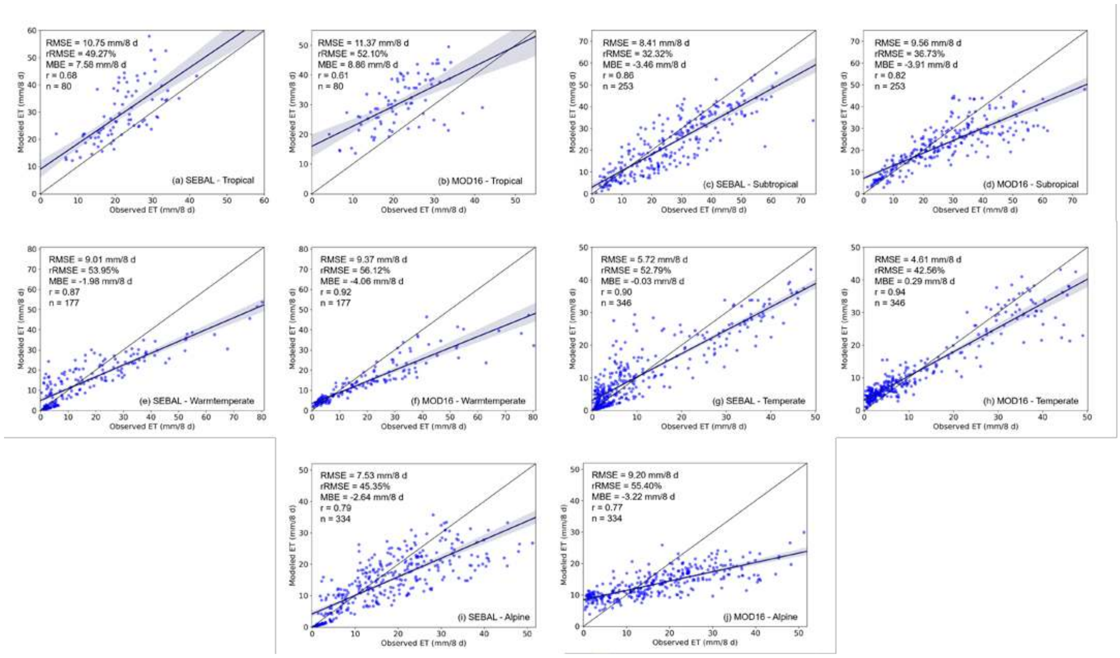

Figure 6. Validations for different climate zones. (a) SEBAL ET for tropical zones; (b) MOD16 ET for tropical zones; (c) SEBAL ET for subtropical zones; (d) MOD16 ET for subtropical zones; (e) SEBAL ET for warm temperate zones; (f) MOD16 ET for warm temperate zones; (g) SEBAL ET for temperate zones; (h) MOD16 ET for temperate zones; (i) SEBAL ET for alpine zones; (j) MOD16 ET for alpine zones.

3.2.3 Performance of the RS-based model over different terrain types

The validation results for different terrain types are shown in Fig. 7. The results indicate that both models showed a negative bias (negative MBE) for all terrain types except mountainous areas, for which both models overestimated, with MBEs of 1.19 and 1.67 mm/8 d for SEBAL and MOD16, respectively. In general, for mountainous areas, MOD16 showed a higher accuracy (RMSE = 7.79 mm/8 d, rRMSE = 41.88%, r = 0.82) than SEBAL (RMSE = 8.37 mm/8 d, rRMSE = 45.06%, r = 0.79). However, for all other terrain types, SEBAL showed a higher accuracy. With SEBAL, the RMSE decreased from 9.01 to 6.51 mm/8 d as elevation increased. For hilly areas, SBEAL showed the lowest rRMSE (32.32%) while MOD16 showed the highest rRMSE (36.73%). For plain areas, SEBAL showed a slightly higher accuracy (RMSE = 9.01 mm/8 d, rRMSE = 53.95%) than MOD16 (RMSE = 9.37 mm/8 d, rRMSE = 56.12%), while for plateau area, SEBAL (RMSE = 6.51 mm/8 d, rRMSE = 52.63%) was more accurate than MOD16 (RMSE = 7.77 mm/8 d, rRMSE = 62.89%).

https://doi.org/10.5194/essd-2020-345
Preprint. Discussion started: 29 December 2020
© Author(s) 2020. CC BY 4.0 License.

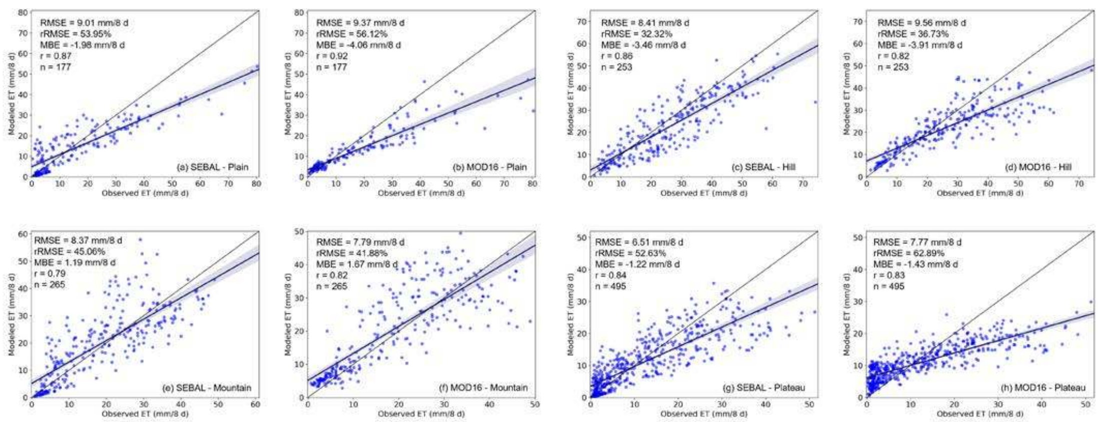

Figure 7. Validation over different terrain: (a) SEBAL ET in plain area; (b) MOD16 ET in plain area; (c) SEBAL ET in hill area; (d) MOD16 ET in hill area; (e) SEBAL ET in mountain area; (f) MOD16 ET in mountain area; (g) SEBAL ET in plateau area; (h) MOD16 ET in plateau area.

3.2.4 Performance of the RS-based model in different seasons

The validation results for different seasons are shown in Fig. 8. SEBAL showed a negative bias in summer, autumn, and winter, with MBE values varying from –2.95 to –0.62 mm/8 d, and showed a positive bias in spring (MBE = 3.13 mm/8 d). MOD16 showed a positive bias in winter (MBE = 3.8 mm/8 d) and a negative bias in other seasons, with MBE values varying from –0.58 to –0.50 mm/8 d. In spring, MOD16 generally showed a better performance (RMSE = 8.10 mm/8 d, rRMSE = 50.13% and r = 0.77) than SEBAL (RMSE = 9.18mm/8 d, rRMSE = 56.92% and r = 0.75), while SEBAL performed better than MOD16 in other seasons. In winter, both the models showed a poor performance, with rRMSEs of 66.92% and 87.80% for SEBAL and MOD16, respectively. For both models, the highest accuracy was achieved in summer, with rRMSEs of 36.56% and 43.95% for SEBAL and MOD16, respectively. Meanwhile, the highest r-values were obtained in autumn, with values of 0.89 and 0.84 for SEBAL and MOD16, respectively.

https://doi.org/10.5194/essd-2020-345
Preprint. Discussion started: 29 December 2020
© Author(s) 2020. CC BY 4.0 License.

Open Access Earth System Science Data Discussions

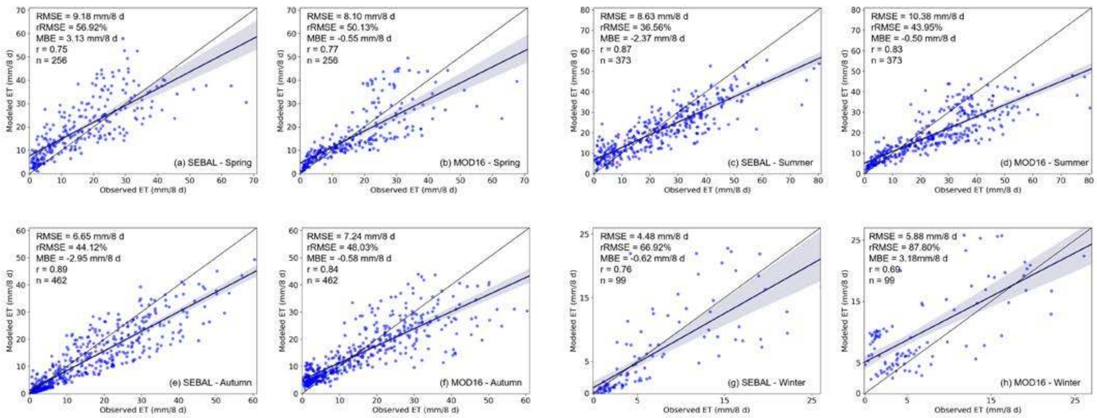

Figure 8. Validation for different seasons. (a) SEBAL ET for spring; (b) MOD16 ET for spring; (c) SEBAL ET for summer; (d) MOD16 ET for summer; (e) SEBAL ET for autumn; (f) MOD16 ET for autumn; (g) SEBAL ET for winter; (h) MOD16 ET for winter.

3.2.5 Summary of point-scale validation

Based on the contents of sections 3.1.1–3.1.4, SEBAL showed a higher accuracy than MOD16 in most conditions, while MOD16 showed a better performance only for temperate zones, mountainous areas, or the spring season based on the values of RMSE and rRMSE. Moreover, both the models underestimated for all conditions, except that SBEAL overestimated for tropical zones (MBE = 7.58 mm/8 d), mountainous areas (MBE = 1.19 mm/8 d), or spring (MBE = 3.13 mm/8 d), and MOD16 overestimated for tropical zones (MBE = 8.86 mm/8 d), temperate zones (MBE = 0.29 mm/8 d), mountainous areas (MBE = 1.67 mm/8 d), or winter (MBE = 3.18 mm/8 d). In general, SEBAL showed a higher accuracy than MOD16 based on point-scale validation (Fig. 9). For SEBAL and MOD16, respectively, the RMSE was 7.77 and 8.43 mm/8 d, the rRMSE was 44.91% and 48.72%, and the r-value was 0.85 and 0.83. Furthermore, both the models slightly underestimated overall, with an MBE of –1.27 and –1.66 mm/8 d for SEBAL and MOD16, respectively.

https://doi.org/10.5194/essd-2020-345
Preprint. Discussion started: 29 December 2020
© Author(s) 2020. CC BY 4.0 License.

Open Access Earth System Science Data Discussions

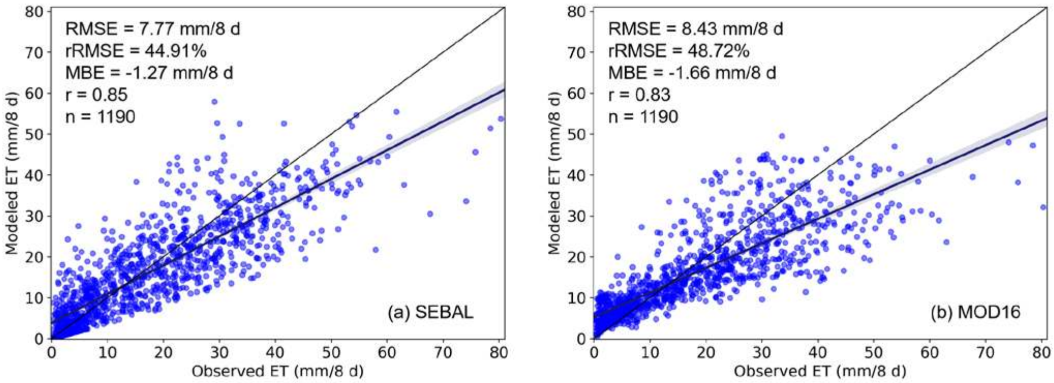

Figure 9. The results of the overall validation. (a) SEBAL ET validation at the 8-day scale; (b) MOD16 ET validation at the 8-day scale.

3.3 Validation at the basin-scale using the water balance method

Additionally, validation using hydrological data was performed to investigate the performance of the RS-based models at the basin-scale. The results (Fig. 10) showed that both the models had a negative bias, with an MBE of –19.17 and –96.66 mm/year for SEBAL and MOD16, respectively, at the basin-scale. SEBAL showed a higher accuracy, with an RMSE of 91.39 mm/year, an rRMSE of 19.15%, and an r-value of 0.88 (MOD16: RMSE = 160.41 mm/year, rRMSE = 33.62%, r = 0.79). As shown in Table 2, the rRMSE of SEBAL varied from 8.93 to 40.25% among the different basins, with this model showing the best performance in the YRB and the worst performance in the CB. The RMSE of SEBAL varied from 35.80 to 188.54 mm/year. The rRMSE of MOD16 varied from 7.26% to 71.59% among the different basins; MOD16 showed the best performance for the SWB and the worst performance for the CB, and the RMSE varied from 29.37 to 274.96 mm/year. In general, both the models performed better at the basin-scale than the point-scale.

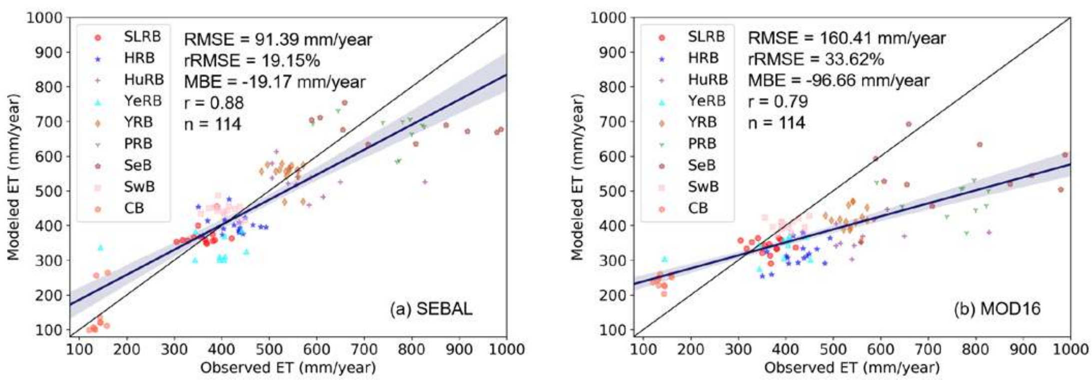

https://doi.org/10.5194/essd-2020-345
Preprint. Discussion started: 29 December 2020
© Author(s) 2020. CC BY 4.0 License.

Figure 10. The results of validation at the basin-scale. (a) SEBAL; (b) MOD16. Note: SwB: Southwest Basin; CB: Continental Basin; PRB: Pearl River Basin; YRB: Yangtze River Basin; SeB: Southeast Basin; HRB: Haihe River Basin; YeRB: Yellow River Basin; HuRB: Huaihe River Basin; SLRB: Songhua and Liaohe River Basin.

Table 2. The performance of the ET estimation of RS-based models at the basin-scale.

Basin	Model	Average (mm/year)	RMSE (mm/year)	rRMSE (%)
SLRB	SEBAL	369.11	35.8	9.91%
	MOD16	339.09	44.26	12.26%
HRB	SEBAL	403.46	55.6	13.11%
	MOD16	319.43	111.72	26.33%
HuRB	SEBAL	535.56	111.28	19.15%
	MOD16	372.45	223.51	38.47%
YeRB	SEBAL	332.92	98.2	26.29%
	MOD16	333.18	86.71	23.21%
YRB	SEBAL	549.04	47.83	8.93%
	MOD16	419.77	122.37	22.84%
PRB	SEBAL	673.91	126.07	16.72%
	MOD16	473.13	295.81	39.22%
SeB	SEBAL	682.22	188.54	24.23%
	MOD16	559.22	274.96	35.34%
SwB	SEBAL	444.27	53.73	13.28%
	MOD16	400.52	29.37	7.26%
CB	SEBAL	141.82	56.36	40.25%
	MOD16	238.44	100.24	71.59%

3.4 Comparison of the spatial distribution of ET between SEBAL and MOD16

Regarding the modeled spatial distribution of ET, both the SEBAL and MOD16 models showed that the annual average (2001–2018) ET in China increased from the northwest to the southeast (Fig. 11(a), (b)). Fig. 11(d). The annual ET of SEBAL varied from 0 to 1600 mm in space, with a mean value of 482.27±192.31 mm, while that of MOD16 varied from 0 to 1200 mm, with a mean value of 359.61±59.52 mm. In general, compared to the ET value estimated using MOD16 and SEBAL, the ET value estimated

https://doi.org/10.5194/essd-2020-345
Preprint. Discussion started: 29 December 2020
© Author(s) 2020. CC BY 4.0 License.

using SEBAL was higher and showed a greater spatial difference of ET in China. For 84.07% of the total area of China, the annual ET estimated by SEBAL was higher than that estimated by MOD16; for 14.07% of the total area of China, the difference was more than two times—these areas are mainly distributed in Southern China, where ET is relatively high, and the difference reaches more than 600 mm in some places. Only in 15.93% of the total area of the country was the annual ET estimated by SEBAL lower than that estimated by MOD16; these areas are mainly distributed in Northwest China, where ET is relatively low (Fig. 11(c), (e)).

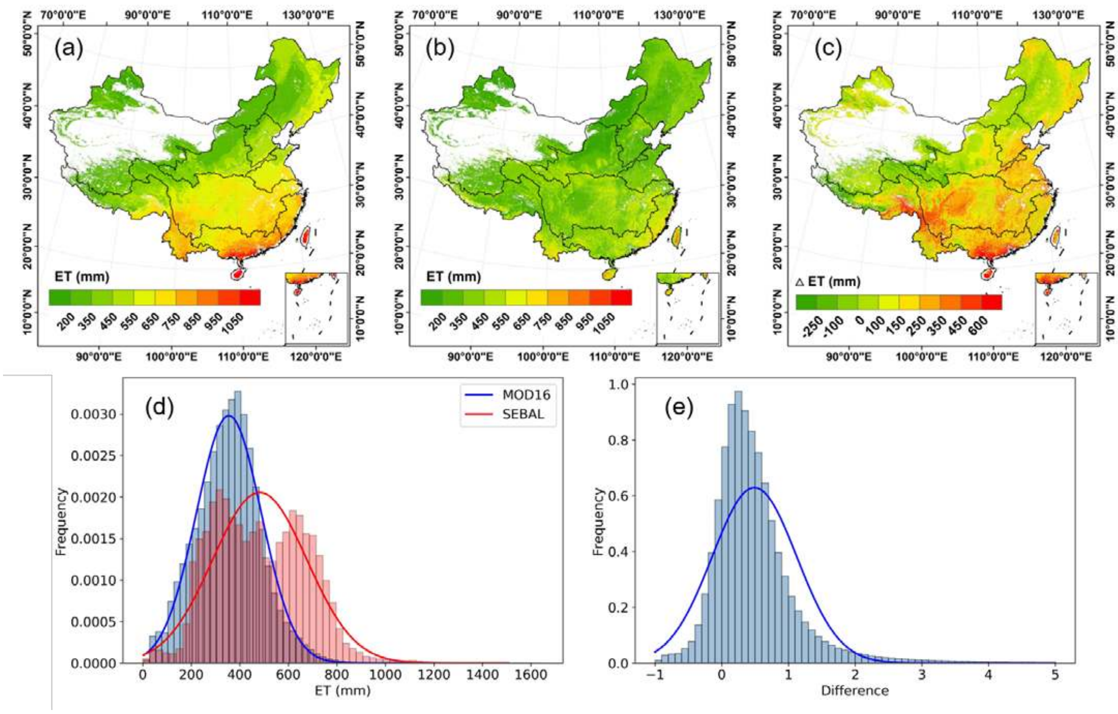

Figure 11. A comparison between the SEBAL and MOD16 models. (a) Distribution of annual average ET_{SEBAL}; (b) Distribution of annual average ET_{MOD}; (c) Distribution of the difference between SEBAL and MOD16 ($ET_{SEBAL} – ET_{MOD}$); (d) Histogram of annual average ET_{SEBAL} and ET_{MOD}; (e) Histogram of the relative difference between SEBAL and MOD16 (($ET_{SEBAL} – ET_{MOD}$)/ET_{MOD}).

4. Discussion

4.1 Summary of validation results and comparison with other studies

The ET_{SEBAL} showed a relatively good performance in China as a whole, with an average r-value of 0.79 and an average RMSE of 0.92 mm/d. These results are close to those obtained in other studies. Rahimzadegan and Janani (2019) used SEBAL to estimate the actual ET of pistachio in Semnan, Iran, and found that the modeled value had a high consistency with the in-situ measured value (r = 0.80); this value was slightly lower than the cropland validation obtained in the present study (r = 0.88, daily-scale). This difference is mainly due to differences in the validation method between these two studies. Rahimzadegan and Janani (2019) used the P-M

https://doi.org/10.5194/essd-2020-345
Preprint. Discussion started: 29 December 2020
© Author(s) 2020. CC BY 4.0 License.

equation and field observational data from Intelligent Meteorological instruments to measure the standard ET, and MOD16 data which is also based on P-M equation was evaluated in this study that performed worse than SEBAL estimation at both point-scale and basin-scale. Xue et al. (2020) used pySEBAL (SEBAL in the Python environment) to estimate the ET of almonds, tomatoes, and maize in the Central Valley of California, USA, and showed that the r-value and RMSE of pySEBAL varied from 0.60 to 0.86 and from 1.08 to 1.79 mm/d, respectively; the authors used Landsat 8 OLI/TIRS images with a spatial resolution of 30 m × 30 m as the model input, which leads to a lower influence of mixed pixels compared to MODIS data with a spatial resolution of 1 km × 1 km. Wagle et al. (2017) evaluated the performance of SEBAL for ET estimation for sorghum based on flux tower observational data from Oklahoma, USA; the results showed that the r-value varied from 0.73 to 0.87 while the RMSE varied from 0.83 to 1.24 mm/d, which is basically in agreement with the results of this study (r-value varied from 0.68 to 0.90 and RMSE varied from 4.48 to 10.75 mm/8 d under different environmental conditions). MOD16 performed worse than SEBAL. Part of the bias is caused by objective factors such as the inaccuracy of the input data and the limitations of the validation methods. Meanwhile, other bias is contributed by the subjective factor of the inborn defects of the algorithms. These factors will be discussed in detail in Sections 4.2 and 4.3.

4.2 Errors caused by objective factors

4.2.1 Inaccuracy of input data

Both SEBAL and MOD16 used MODIS data as the main input images (e.g., MCD43 surface albedo, MOD13 NDVI, MOD11 surface temperature). However, the accuracy of these data is uncertain to some extent (Ramoelo et al., 2014). For instance, surface albedo is a critical radiative parameter, however, the complex algorithm-led remote sensing-based albedo products can contain errors introduced by the spectral conversion (Song et al., 2020). Wang et al. (2014) compared MODIS albedo products with ground data and Landsat data for different land cover types in the USA, and found that the RMSE of the products varied from 0.01–0.05 and that the error was higher during periods of snow cover. Furthermore, surface temperature, as a fundamental parameter for the calculation of surface energy balance, affected the estimation of ET to a great extent (Long et al., 2011). Timmermans et al. (2006) analyzed the sensitivity of each parameter of the SEBAL model to grassland in Oklahoma, USA, and the results indicated that the difference in surface air temperature had the greatest influence on the accuracy of SEBAL estimation. MODIS surface temperature products are retrieved using the split-window algorithm. Yu et al. (2019) used in-situ measurement data to validate MODIS surface temperature products in the Heihe River Basin (HRB) in Northwest China; the results indicated that the daytime MOD11 (obtained by the Terra satellite) and MYD11 (obtained by the Aqua satellite) products have accuracies of –0.84±0.88 K and –0.11±0.42 K, respectively. Additionally, Heinsch et al. (2006) evaluated the influence of GMAO meteorological data on the estimation of GPP, and showed that the error of GPP computed from GMAO reached 28%. Therefore, the GMAO data were not accurate enough.

https://doi.org/10.5194/essd-2020-345
Preprint. Discussion started: 29 December 2020
© Author(s) 2020. CC BY 4.0 License.

4.2.2 Errors in flux tower measurements

The eddy covariance system (flux tower observations) is the most commonly used observation system to calculate and analyze the energy and mass exchange between the surface and atmosphere (Wang and Dickinson, 2012). However, the typical error of ET estimation based on the eddy covariance system is about 5–20% (Culf et al., 2008; Vickers et al., 2010). In this study, the results of the point-scale validation based on flux tower observations showed that the rRMSE of SEBAL varied from 32.32% to 66.92% and that of MOD16 varied from 36.73% to 87.80%. Compared to the basin-scale validation based on a water balance method, which is simpler and more direct than the point-scale validation, the rRMSE was 19.15% for SEBAL and 33.62% for MOD16, and both the models showed a lower bias at the basin-scale. The poor point-scale validation of the RS-based models may be partly due to the error of the flux tower observations. Furthermore, the spatial range (footprint) of the flux tower observational data is not consistent with the spatial resolution of the RS-based models. In a study in Asia, Kim et al. (2012) resampled the MOD16 product to 3 km × 3 km to match the footprint of the flux tower data. Velpuri et al. (2013) used ET estimated using MOD16 and the Operational Simplified Surface Energy Balance (SSEBop) with a spatial resolution of 1 km × 1 km to match the footprint of the flux tower data in the USA. Several studies have indicated that the footprint should be determined by the height of the observation instrument and the intensity of the turbulence (Damm et al., 2020; Schmid, 1994). It should be noted that the footprint of the flux tower data used in this study varied with the meteorological conditions. Therefore, the inconsistency between the footprint of the in-situ measurements and the modeled data will cause errors in the validation process.

4.3 Errors caused by subjective factors

4.3.1 Temporal scaling-up method

Remotely sensed information represents the information of satellite-passing time. Therefore, in the RS-based models, scaling-up was performed from the instantaneous level to the daily level. SEBAL uses the evaporative fraction (Λ) for scaling-up (Gao et al., 2020), as shown in Eqs. 32 and 33. However, several studies have indicated that the assumption of a constant evaporative fraction is not reasonable (Gentine et al., 2011; Hoedjes et al., 2008). Gentine et al. (2007) proposed that soil moisture and vegetation resistance are the factors that mainly affect the stability of Λ, and soil moisture is positively correlated with Λ. Additionally, a larger leaf area index will generally lead to a lower stability of Λ under the same soil moisture (Farah et al., 2004). In general, due to the instability of Λ, the above assumption will cause a negative bias of 10–20% in the estimation of daily ET (Delogu et al., 2012; Ryu et al., 2012; Van Niel et al., 2012). This can explain why the validation in this paper showed that the ET estimated using SEBAL was underestimated. While the MOD16 model estimates daily ET using the P-M equation, which is a semi-empirical equation, it uses 8-day or 16-day composite remotely sensed input data and daily meteorological input data to compute the 8-day composite ET products (Mu et al., 2011). The use of a semi-empirical equation avoids the need to perform scaling-up, however, it has the problem

https://doi.org/10.5194/essd-2020-345
Preprint. Discussion started: 29 December 2020
© Author(s) 2020. CC BY 4.0 License.
Open Access Earth System Science Data Discussions

of theoretical deficiency (Mu et al., 2007; Ramoelo et al., 2014).

4.3.2 Classification of ET

The MOD16 model (a model based on the P-M equation) divides surface ET into three parts: evaporation from wet canopy surface (ET_{wet_c}), plant transpiration (ET_{trans}), and evaporation from the soil surface (ET_{soil}) (Eqs. 40–42); the daily ET is calculated as the sum of these three parts (Mu et al., 2011).

$$\lambda ET_{wet\_c} = \frac{(sA_c F_c + \rho C_p VPD F_c / r_a) F_{wet}}{s + P_a C_p (r_s + r_a) / \lambda r_a} \tag{40}$$

$$\lambda ET_{trans} = \frac{(sA_c F_c + \rho C_p VPD F_c / r_a)(1 - F_{wet})}{s + \gamma (1 + r_s / r_a)} \tag{41}$$

$$\begin{aligned} \lambda ET_{soil} &= \lambda ET_{wet\_soil} + \lambda ET_{pot\_soil} + \left(\frac{RH}{100}\right)^{VPD/\beta} \\ &= \frac{(sA_{soil} + \rho C_p VPD(1 - F_c) / r_{as}) F_{wet}}{s + \gamma r_{tot} / r_{as}} + \frac{(sA_{soil} + \rho C_p VPD(1 - F_c) / r_{as})(1 - F_{wet})}{s + \gamma r_{tot} / r_{as}} + \left(\frac{RH}{100}\right)^{VPD/\beta} \end{aligned} \tag{42}$$

where A_c and A_{soil} (unit: W/m^2) are the parts of the available energy allocated to the vegetation canopy and soil surface, respectively; F_c is the vegetation cover fraction; F_{wet} is the water cover fraction, which is calculated using the relative humidity (RH, unit: %); P_a (unit: Pa) is atmospheric pressure; ET_{wet_soil} and ET_{pot_soil} (unit: mm) are the wet soil evaporation and potential soil evaporation, respectively; β is a constant, which is given a value of 200 (Mu et al., 2011); r_{tot} (unit: s/m) is the aerodynamic resistance to vapor transport; and r_{as} (unit: s/m) is the boundary-layer resistance. Unlike in the MOD16 model, in the SEBAL model, the soil evaporation and vegetation transpiration are calculated as a whole in the form of latent heat. This may explain why, in the present study, MOD16 performed better in conditions with more mixed pixels, such as in mountainous areas and the spring season. However, due to the theoretical deficiency of the P-M algorithm, the performance of MOD16 was worse than that of SEBAL in most conditions. Furthermore, two-source SEB-based models distinguish vegetation and soil to calculate aerodynamic resistance (Long and Singh, 2012; Yang and Shang, 2013). Several studies have compared one-source SEB-based models with two-source SEB-based models, and the results indicated that these two types of model performed differently in different conditions (French et al., 2015; Xia et al., 2016). However, there is no evidence that two-source SEB-based models have better performance than one-source SEB-based models.

4.3.3 Calculation of sensible heat flux

Sensible heat flux is the most complicated part of the energy balance calculation (Wang and Dickinson, 2012). The P-M algorithm

https://doi.org/10.5194/essd-2020-345
Preprint. Discussion started: 29 December 2020
© Author(s) 2020. CC BY 4.0 License.

defines the available energy (A, unit: W/m^2) as the sum of the sensible heat flux and latent heat flux (Eq. 43) (Mu et al., 2011).

$$A = H + \lambda ET = R_n - G \tag{43}$$

The P-M algorithm calculates λET using a semi-empirical formula and A, and therefore avoids the direct calculation of H. Meanwhile, SEBAL calculates H based on MOST and the warmest and coldest spots (Bastiaanssen et al., 1998a; Bastiaanssen et al., 1998b). However, several studies have indicated that MOST has an error of 10–20% for the estimation of the boundary layer thickness (Foken, 2006; Högström and Bergström, 1996). Therefore, MOST is also a source of error in SEBAL. Due to the complexity of the sensible heat flux, SEBAL makes several assumptions to estimate H, which may introduce error into the ET estimation (Zheng et al., 2016). Furthermore, the selection of the warmest and coldest spots depends on the domain size (Long et al., 2011). For instance, the basin-scale selection of the warmest and coldest spots with diverse vegetation cover and single vegetation cover, respectively, will lead to different results for dT, which may explain why SEBAL performed the worst in spring, which has low vegetation cover and a low domain size. This method for the estimation of H has an accuracy of ~50 W/m^2 (Seguin et al., 1999). Although several algorithms have been proposed that use other methods to avoid the error caused by the selection of the warmest and coldest spots, such as the SEBS (Su, 1999), these replaced the selection of the warmest and coldest spots with the fitting of dry and wet edges. However, no evidence has been found that the method of fitting dry and wet edges can significantly improve the accuracy of ET estimation (Wagle et al., 2017; Xue et al., 2020).

5. Data availability

The dataset that was generated using SEBAL with a spatial resolution of 1 km and a temporal resolution of 1 day can be used for various types of geoscientific studies, especially for global change, water resources management, agricultural drought monitoring, etc. The evapotranspiration (ET) dataset for China is distributed under a Creative Commons Attribution 4.0 International license. The dataset is named SEBAL evapotranspiration in China (SEBAL ET) and consists of 18 years of data. More information and data are freely available from the Zenodo repository at https://doi.org/ 10.5281/zenodo.4218413 (Cheng, 2020).

6. Conclusions

In this study, we generated a long time series (2001–2018) ET product based on SEBAL and multisource images. We further conducted a comprehensive validation of the product and compared its performance under different environmental conditions in China with the performance of the ET estimated using MOD16 data. The conclusions are as follows:

(1) The ET product generated using SEBAL showed a good performance in China. Compared to flux tower observational data, the r-value of the SEBAL ET reached 0.79 for 9896 samples; the RMSE was 0.92 mm/d and the rRMSE was 42.04%. SEBAL

underestimated ET as whole, with an MBE of –0.15 mm/d. The SEBAL ET product can adequately represent the actual ET and can be used in research on water resources management, drought monitoring, ecological change, etc.

(2) Based on observational data from eight flux towers from 2003 to 2010, the ET datasets estimated using SEBAL and MOD16 were validated at the 8-day scale for different land cover types, climate zones, terrain types, and seasons. The results showed that SEBAL performed best in the conditions of forest cover (rRMSE = 38.08%), subtropical zones (rRMSE = 32.32%), hilly terrain (rRMSE = 32.32%), and the summer season (rRMSE = 36.56%), respectively, and performed worst in the conditions of grassland cover (rRMSE = 52.63%), warm-temperate zones (rRMSE = 53.95%), plain terrain (rRMSE = 53.95%), and the winter season (rRMSE = 66.92%), respectively; MOD16 performed best in the conditions of forest cover (rRMSE = 39.29%), subtropical zones (rRMSE = 36.73%), hilly terrain (rRMSE = 36.73%), and the summer season (rRMSE = 43.95%), respectively, and performed worst in the conditions of grassland cover (rRMSE = 62.89%), warm-temperate zones (rRMSE = 52.10%), plateau terrain (rRMSE = 62.89%), and the winter season (rRMSE = 87.80%), respectively. In general, the two models have similar adaptability to different conditions, although SEBAL performed slightly better than MOD16.

(3) Based on flux tower observational data and hydrological observational data, the ET estimated by SEBAL and MOD16 were validated at the point-scale and basin-scale. The results showed that, at the point-scale, the accuracy of SEBAL was 7.77 mm/8 d for the RMSE, 44.91% for the rRMSE, and 0.85 for the r-value, and the accuracy of MOD16 was 8.43 mm/8 d for the RMSE, 48.72% for the rRMSE, and 0.83 for the r-value. At the basin-scale, the accuracy of SEBAL was 91.39 mm/year for the RMSE, 19.15% for the rRMSE, and 0.88 for the r-value. SEBAL performed best in the YRB (rRMSE = 8.93%) and worst in the CB (rRMSE = 40.25%). At the basin-scale, the accuracy of MOD16 was 160.41 mm/year for the RMSE, 33.62% for the rRMSE, and 0.85 for the r-value. MOD16 performed best in the SWB (rRMSE = 7.26%) and worst in the CB (rRMSE = 71.59%). Moreover, both the models showed a negative bias at all scales of validation. In general, SEBAL performed slightly better than MOD16 at the point-scale, while SEABAL had a larger accuracy advantage at the basin-scale.

(4) Overall, the SEBAL ET is higher than the MOD16 ET: for 84.07% of the total area of China, the SEBAL ET showed higher values. Additionally, the SEBAL ET is closer to the in-situ measured ET in most conditions, while the MOD16 ET performed better only in temperate zones, mountain areas, or the spring season. In general, the two models both have a good performance and can be used in the qualitative analysis and most quantitative analysis of regional ET. Furthermore, the combination of the two models can improve the overall ET estimation accuracy for use in applications with higher accuracy requirements.

Compared the widely used MOD16 ET data, the SEBAL ET product showed a higher accuracy and temporal resolution. However, it still has a daily error of 42.04% (0.92 mm/d) at the point-scale and a yearly error of 19.15% (91.39 mm/year) at the basin-scale. Therefore, the improvement of the SEBAL algorithm will be the focus of follow-up research. Moreover, the 1 km spatial resolution of the SEBAL ET product cannot meet the requirements of more detailed research. Due to the difficulty of simultaneously satisfying the requirements for the spatial and temporal resolutions of remote sensing data, the fusion of multiple sources of remote sensing data may be the most effective way to improve the spatiotemporal resolution of daily ET products.

Acknowledgements:

This study was financially supported by the National Key Research and Development Program of China (2016YFD0300605).

Conflict of interest statement:

The authors declare no conflict of interest.

https://doi.org/10.5194/essd-2020-345
Preprint. Discussion started: 29 December 2020
© Author(s) 2020. CC BY 4.0 License.

Open Access Earth System Science Data Discussions

References:

Bastiaanssen, W.G.M., Menenti, M., Feddes, R.A., & Holtslag, A.A.M.: A remote sensing surface energy balance algorithm for land (SEBAL). 1. Formulation. Journal of Hydrology, 21210.1016/s0022-1694(98)00253-4, 1998a.

Bastiaanssen, W.G.M., Pelgrum, H., Wang, J., Ma, Y., Moreno, J.F., Roerink, G.J., & Wal, T.V.D.: A remote sensing surface energy balance algorithm for land (SEBAL): 2. Validation. Journal of Hydrology, 21210.1016/S0022-1694(98)00254-6, 1998b.

Bastiaanssen, W.G.M., & Steduto, P.: The water productivity score (WPS) at global and regional level: Methodology and first results from remote sensing measurements of wheat, rice and maize. The Science of the total environment, 57510.1016/j.scitotenv.2016.09.032, 2017.

Carlson, T.: An Overview of the "Triangle Method" for Estimating Surface Evapotranspiration and Soil Moisture from Satellite Imagery. Sensors, 7(8), 17, doi:10.3390/s7081612, 2007.

Chen, X., Su, Z., Ma, Y., Liu, S., Yu, Q., & Xu, Z.: Development of a 10-year (2001–2010) 0.1° data set of land-surface energy balance for mainland China. Atmospheric Chemistry and Physics, 14, 14471-14518, 10.5194/acp-14-13097-2014, 2014.

Chen, X.L.: A column canopy-air turbulent diffusion method for different canopy structures. Journal of Geophysical Research: Atmospheres, 124, 18, 10.1029/2018jd028883 2019.

Cheng, M.: Long time series (2001-2018) of daily evapotranspiration in China generated based on SEBAL (Version 1.0) [Data set]. Zenodo.10.5281/zenodo.4218413, 2020.

Crago, R.D.: Conservation and variability of the evaporative fraction during the daytime Journal of Hydrology, 18010.1016/0022-1694(95)02903-6, 1996.

Culf, A.D., Foken, T., & Gash, J.H.C.: The energy balance closure problem: an overview. Ecological Applications, 18, 1351-1367, 10.1890/06-0922.1, 2008.

Damm, A., Paul-Limoges, E., Kukenbrink, D., Bachofen, C., & Morsdorf, F.: Remote sensing of forest gas exchange: Considerations derived from a tomographic perspective. Global Change Biology10.1111/gcb.15007, 2020.

Delogu, E., Boulet, G., Olioso, A., Coudert, B., Chirouze, J., Ceschia, E., Le Dantec, V., Marloie, O., Chehbouni, G., & Lagouarde, J.P.: Reconstruction of temporal variations of evapotranspiration using instantaneous estimates at the time of satellite overpass. Hydrology and Earth System Sciences, 16, 2995-3010, 10.5194/hess-16-2995-2012, 2012.

Elnmer, A., Khadr, M., Kanae, S., & Tawfik, A.: Mapping daily and seasonally evapotranspiration using remote sensing techniques over the Nile delta. Agricultural Water Management, 213, 682-692, 10.1016/j.agwat.2018.11.009, 2019.

Farah, H.O., Bastiaanssen, W.G.M., & Feddes, R.A.: Evaluation of the temporal variability of the evaporative fraction in a tropical watershed. International Journal of Applied Earth Observation and Geoinformation, 5, 129-140, 10.1016/j.jag.2004.01.003, 2004.

Foken, T.: 50 years of the Monin–Obukhov similarity theory. Boundary-Layer Meteorology, 119, 431-447, 10.1007/s10546-006-

9048-6, 2006.

French, A.N., Hunsaker, D.J., & Thorp, K.R.: Remote sensing of evapotranspiration over cotton using the TSEB and METRIC energy balance models. Remote Sensing of Environment, 158, 281-294, 2015.

Gao, X.R., Sun, M., Luan, Q.H., Zhao, X.N., Wang, J.C., He, G.H., & Zhao, Y.: The spatial and temporal evolution of the actual evapotranspiration based on the remote sensing method in the Loess Plateau. Science of the Total Environment, 70810.1016/j.scitotenv.2019.135111 2020.

Gentine, P., Entekhabi, D., Chehbouni, A., Boulet, G., & Duchemin, B.: Analysis of evaporative fraction diurnal behaviour. Agricultural and Forest Meteorology, 143, 13-29, 10.1016/j.agrformet.2006.11.002, 2007.

Gentine, P., Entekhabi, D., & Polcher, J.: The Diurnal Behavior of Evaporative Fraction in the Soil–Vegetation–Atmospheric Boundary Layer Continuum. Journal of Hydrometeorology, 12, 1530-1546, 10.1175/2011JHM1261.1, 2011.

Gobbo, Presti, Martello, Panunzi, Berti, & Morari: Integrating SEBAL with in-Field Crop Water Status Measurement for Precision Irrigation Applications—A Case Study. Remote Sensing, 1110.3390/rs11172069, 2019.

Högström, U., & Bergström, H.: Organized turbulence structures in the near-neutral atmospheric surface layer. Journal of the Atmospheric Sciences, 53, 2452-2464, 10.1029/2004GL019935, 1996.

He, M., Kimball, J.S., Yi, Y., Running, S.W., Guan, K., Moreno, A., Wu, X., & Maneta, M.: Satellite data-driven modeling of field scale evapotranspiration in croplands using the MOD16 algorithm framework. Remote Sensing of Environment, 23010.1016/j.rse.2019.05.020, 2019.

Heinsch, F.A., Zhao, M., Running, S.W., Kimball, J.S., & Nemani, R.R.: Evaluation of remote sensing based terrestrial productivity from MODIS using AmeriFlux tower eddy flux network observations IEEE Transactions on Geoscience and Remote Sensing, 4410.1109/TGRS.2005.853936, 2006.

Helbig, M., Waddington, J.M., Alekseychik, P., Amiro, B.D., Aurela, M., Barr, A.G., Black, T.A., Blanken, P.D., Carey, S.K., Chen, J., Chi, J., Desai, A.R., Dunn, A., Euskirchen, E.S., Flanagan, L.B., Forbrich, I., Friborg, T., Grelle, A., Harder, S., Heliasz, M., Humphreys, E.R., Ikawa, H., Isabelle, P.-E., Iwata, H., Jassal, R., Korkiakoski, M., Kurbatova, J., Kutzbach, L., Lindroth, A., Löfvenius, M.O., Lohila, A., Mammarella, I., Marsh, P., Maximov, T., Melton, J.R., Moore, P.A., Nadeau, D.F., Nicholls, E.M., Nilsson, M.B., Ohta, T., Peichl, M., Petrone, R.M., Petrov, R., Prokushkin, A., Quinton, W.L., Reed, D.E., Roulet, N.T., Runkle, B.R.K., Sonnentag, O., Strachan, I.B., Taillardat, P., Tuittila, E.-S., Tuovinen, J.-P., Turner, J., Ueyama, M., Varlagin, A., Wilmking, M., Wofsy, S.C., & Zyrianov, V.: Increasing contribution of peatlands to boreal evapotranspiration in a warming climate. Nature Climate Change, 10, 555-560, 10.1038/s41558-020-0763-7, 2020.

Hoedjes, J.C.B., Chehbouni, A., Jacob, F., Ezzahar, J., & Boulet, G.: Deriving daily evapotranspiration from remotely sensed instantaneous evaporative fraction over olive orchard in semi-arid Morocco. Journal of Hydrology, 354, 53-64, 10.1016/j.jhydrol.2008.02.016, 2008.

https://doi.org/10.5194/essd-2020-345
Preprint. Discussion started: 29 December 2020
© Author(s) 2020. CC BY 4.0 License.

Huang, C., Li, Y., Gu, J., Lu, L., & Li, X.: Improving Estimation of Evapotranspiration under Water-Limited Conditions Based on SEBS and MODIS Data in Arid Regions. Remote Sensing, 7info:doi/10.3390/rs71215854, 2015.

Jaafar, H.H., & Ahmad, F.A.: Time series trends of Landsat-based ET using automated calibration in METRIC and SEBAL: The Bekaa Valley, Lebanon. Remote Sensing of Environment, 23810.1016/j.rse.2018.12.033, 2020.

Jin, X., Li, Z., Feng, H., Ren, Z., & Li, S.: Deep neural network algorithm for estimating maize biomass based on simulated Sentinel 2A vegetation indices and leaf area index. The Crop Journal, 8, 87-97, 10.1016/j.cj.2019.06.005, 2020.

Karimi, P., & Bastiaanssen, W.G.M.: Spatial evapotranspiration, rainfall and land use data in water accounting – Part 1: Review of the accuracy of the remote sensing data. Hydrology and Earth System Sciences, 1910.5194/hess-19-507-2015, 2015.

Kim, H.W., Hwang, K., Mu, Q., Lee, S.O., & Choi, M.: Validation of MODIS 16 global terrestrial evapotranspiration products in various climates and land cover types in Asia. KSCE Journal of Civil Engineering, 1610.1007/s12205-012-0006-1, 2012.

Kustas, W.P., Bindlish, R., French, A.N., & Schmugge, T.J.: Comparison of energy balance modeling schemes using microwave-derived soil moisture and radiometric surface temperature. Water Resources Research, 3910.1029/2002wr001361, 2003.

Li, X., Cheng, G., Ge, Y., Li, H., Han, F., Hu, X., Tian, W., Tian, Y., Pan, X., Nian, Y., Zhang, Y., Ran, Y., Zheng, Y., Gao, B., Yang, D., Zheng, C., Wang, X., Liu, S., & Cai, X.: Hydrological Cycle in the Heihe River Basin and Its Implication for Water Resource Management in Endorheic Basins. Journal of Geophysical Research: Atmospheres, 123, 890-914, 10.1002/2017jd027889, 2018.

Long, D., & Singh, V.P.: A Two-source Trapezoid Model for Evapotranspiration (TTME) from satellite imagery. Remote Sensing of Environment, 121, 370-388, 10.1016/j.rse.2012.02.015, 2012.

Long, D., Singh, V.P., & Li, Z.-L.: How sensitive is SEBAL to changes in input variables, domain size and satellite sensor? Journal of Geophysical Research: Atmospheres, 11610.1029/2011jd016542, 2011.

Mhawej, M., Caiserman, A., Nasrallah, A., Dawi, A., Bachour, R., & Faour, G.: Automated evapotranspiration retrieval model with missing soil-related datasets: The proposal of SEBALI. Agricultural Water Management, 22910.1016/j.agwat.2019.105938 2020.

Miralles, D.G., Holmes, T.R.H., De Jeu, R.A.M., Gash, J.H., Meesters, A.G.C.A., & Dolman, A.J.: Global land-surface evaporation estimated from satellite-based observations. Hydrology and Earth System Sciences, 15, 453-469, 10.5194/hess-15-453-2011, 2011.

Miralles, D.G., Holmes, T.R.H., De, J.R.A.M., Gash, J.H., Meesters, A.G.C.A., & Dolman, A.J.: Global land-surface evaporation estimated from satellite-based observations. Hydrology and Earth System Sciences, 7, 453-469, 10.5194/hess-15-453-2011, 2010.

Monin, A.S., & Obukhov, A.M.: Basic laws of turbulent mixing in the surface layer of the atmosphere. Contrib. Geophys. Inst. Acad. Sci. USSR, 151, e187, 1954.

Monteith, J.L.: Evaporation and environment. The stage and movement of water in living organisms. Symp.soc.exp.biol.the Company of Biologists1965.

Moran, M.S., & Jackson, R.D.: Assessing the spatial distribution of evapotranspiration using remotely sensed inputs. Journal of

https://doi.org/10.5194/essd-2020-345
Preprint. Discussion started: 29 December 2020
© Author(s) 2020. CC BY 4.0 License.

Environmental Quality, 20, 725-737, 1991.

Mu, Q., Heinsch, F.A., Zhao, M., & Running, S.W.: Development of a global evapotranspiration algorithm based on MODIS and global meteorology data. Remote Sensing of Environment, 11110.1016/j.rse.2007.04.015 2007.

Mu, Q., Zhao, M., & Running, S.W.: Improvements to a MODIS global terrestrial evapotranspiration algorithm. Remote Sensing of Environment, 11510.1016/j.rse.2011.02.019 2011.

Pôças, I., Calera, A., Campos, I., & Cunha, M.: Remote sensing for estimating and mapping single and basal crop coefficientes: A review on spectral vegetation indices approaches. Agricultural Water Management, 23310.1016/j.agwat.2020.106081, 2020.

Paulson, C.A.: The Mathematical Representation of Wind Speed and Temperature Profiles in the Unstable Atmospheric Surface Layer. J.appl.meteorol, 9, 857-861, 10.1175/1520-0450(1970)0092.0.CO;2, 1970.

Rahimzadegan, M., & Janani, A.: Estimating evapotranspiration of pistachio crop based on SEBAL algorithm using Landsat 8 satellite imagery. Agricultural Water Management, 217, 383-390, 10.1016/j.agwat.2019.03.018, 2019.

Ramoelo, A., Majozi, N., Mathieu, R., Jovanovic, N., Nickless, A., & Dzikiti, S.: Validation of Global Evapotranspiration Product (MOD16) using Flux Tower Data in the African Savanna, South Africa. Remote Sensing, 610.3390/rs6087406, 2014.

Roerink, G.J., Su, Z., & Menenti, M.: S-SEBI: A simple remote sensing algorithm to estimate the surface energy balance. Physics and Chemistry of the Earth, Part B: Hydrology, Oceans and Atmosphere, 25, 147-157, 10.1016/S1464-1909(99)00128-8, 2000.

Ryu, Y., Baldocchi, D.D., Black, T.A., Detto, M., Law, B.E., Leuning, R., Miyata, A., Reichstein, M., Vargas, R., & Ammann, C.: On the temporal upscaling of evapotranspiration from instantaneous remote sensing measurements to 8-day mean daily-sums. Agricultural and Forest Meteorology, 152, 212-222, 10.1016/j.agrformet.2011.09.010, 2012.

Schmid, H.P.: Source areas for scalars and scalar fluxes. Boundary Layer Meteorology, 67, 293-318, 10.1007/BF00713146, 1994.

Seguin, B., Becker, F., Phulpin, T., Gu, X.F., Guyot, G., Kerr, Y., King, C., Lagouarde, J.P., Ottlé, C., & Stoll, M.P.: IRSUTE:A Minisatellite Project for Land Surface Heat Flux Estimation from Field to Regional Scale. Remote Sensing of Environment, 68, 357-369, 1999.

Senay, G.B., Kagone, S., & Velpuri, N.M.: Operational Global Actual Evapotranspiration: Development, Evaluation and Dissemination. Sensors (Basel), 2010.3390/s20071915, 2020.

Smith, M., Allen, R., Monteith, J., Perrier, A., Pereira, L., & Segeren, A.: Report on the expert consultation on procedures for revision of FAO guidelines for prediction of crop water requirements. Rome: FAO1991.

Song, R., Muller, J.-P., Kharbouche, S., Yin, F., Woodgate, W., Kitchen, M., Roland, M., Arriga, N., Meyer, W., Koerber, G., Bonal, D., Burban, B., Knohl, A., Siebicke, L., Buysse, P., Loubet, B., Leonardo, M., Lerebourg, C., & Gobron, N.: Validation of Space-Based Albedo Products from Upscaled Tower-Based Measurements Over Heterogeneous and Homogeneous Landscapes. Remote Sensing, 1210.3390/rs12050833, 2020.

Su, Z.: The Surface Energy Balance System (SEBS) for estimation of turbulent heat fluxes. Hydrology and Earth System Sciences, 610.5194/hess-6-85-2002, 1999.

Tasumi, M.: Application of the SEBAL methodology for estimating consumptive use of water and stream flow depletion in the Bear River Basin of Idaho through remote sensing. Appendix C: a step-by-step guide to running SEBAL2000.

Timmermans, W.J., Kustas, W.P., Anderson, M.C., & French, A.N.: An intercomparison of the Surface Energy Balance Algorithm for Land (SEBAL) and the Two-Source Energy Balance (TSEB) modeling schemes. Remote Sensing of Environment, 10810.1016/j.rse.2006.11.028, 2006.

Van Niel, T.G., McVicar, T.R., Roderick, M.L., van Dijk, A.I.J.M., Beringer, J., Hutley, L.B., & van Gorsel, E.: Upscaling latent heat flux for thermal remote sensing studies: Comparison of alternative approaches and correction of bias. Journal of Hydrology, 468-469, 35-46, 10.1016/j.jhydrol.2012.08.005, 2012.

Velpuri, N.M., Senay, G.B., Singh, R.K., Bohms, S., & Verdin, J.P.: A comprehensive evaluation of two MODIS evapotranspiration products over the conterminous United States: Using point and gridded FLUXNET and water balance ET. Remote Sensing of Environment, 13910.1016/j.rse.2013.07.013, 2013.

Vickers, D., Göckede, M., & Law, B.E.: Uncertainty estimates for 1-h averaged turbulence fluxes of carbon dioxide, latent heat and sensible heat. Tellus, 62, 87-99, 10.1111/j.1600-0889.2009.00449.x, 2010.

Vuolo, F., Ng, W.-T., & Atzberger, C.: Smoothing and gap-filling of high resolution multi-spectral time series: Example of Landsat data. International Journal of Applied Earth Observation and Geoinformation, 57, 202-213, 10.1016/j.jag.2016.12.012, 2017.

Wagle, P., Bhattarai, N., Gowda, P.H., & Kakani, V.G.: Performance of five surface energy balance models for estimating daily evapotranspiration in high biomass sorghum. ISPRS Journal of Photogrammetry and Remote Sensing, 128, 192-203, 10.1016/j.isprsjprs.2017.03.022, 2017.

Wagle, P., Gowda, P.H., & Northup, B.K.: Dynamics of evapotranspiration over a non-irrigated alfalfa field in the Southern Great Plains of the United States. Agricultural Water Management, 223, 105727, 10.1016/j.agwat.2019.105727, 2019.

Wang, K., & Dickinson, R.E.: A review of global terrestrial evapotranspiration: Observation, modeling, climatology, and climatic variability. Reviews of Geophysics, 5010.1029/2011RG000373, 2012.

Wang, Z., Schaaf, C.B., Strahler, A.H., Chopping, M.J., Román, M.O., Shuai, Y., Woodcock, C.E., Hollinger, D.Y., & Fitzjarrald, D.R.: Evaluation of MODIS albedo product (MCD43A) over grassland, agriculture and forest surface types during dormant and snow-covered periods. Remote Sensing of Environment, 140, 60-77, 10.1016/j.rse.2013.08.025, 2014.

Xia, T., Kustas, W.P., Anderson, M.C., Alfieri, J.G., Gao, F., Lynn, M.K., Prueger, J.H., Geli, H.M.E., Neale, C.M.U., & Luis, S.: Mapping evapotranspiration with high-resolution aircraft imagery over vineyards using one- and two-source modeling schemes. Hydrology and Earth System Sciences, 12, 11905-11957, 10.5194/hess-20-1523-2016, 2016.

Xue, J., Bali, K.M., Light, S., Hessels, T., & Kisekka, I.: Evaluation of remote sensing-based evapotranspiration models against surface renewal in almonds, tomatoes and maize. Agricultural Water Management, 23810.1016/j.agwat.2020.106228, 2020.

https://doi.org/10.5194/essd-2020-345
Preprint. Discussion started: 29 December 2020
© Author(s) 2020. CC BY 4.0 License.

Yang, Y., & Shang, S.: A hybrid dual-source scheme and trapezoid framework-based evapotranspiration model (HTEM) using satellite images: Algorithm and model test. Journal of Geophysical Research: Atmospheres, 118, 2284-2300, 10.1002/jgrd.50259, 2013.

Yu, W., Ma, M., Yang, H., Tan, J., & Li, X.: Supplement of the radiance-based method to validate satellite-derived land surface temperature products over heterogeneous land surfaces. Remote Sensing of Environment, 23010.1016/j.rse.2019.05.007, 2019.

Zeng, L., Song, K., Zhang, B., & Du, J.: Applying Landsat Data and SEBAL Model to Inverse Regional Evapotranspiration and Its Parameters Estimation. Remote Sensing Technology and Application, 255-263, 2008.

Zhang, Z., Chen, X., Xu, C.-Y., Yuan, L., Yong, B., & Yan, S.: Evaluating the non-stationary relationship between precipitation and streamflow in nine major basins of China during the past 50 years. Journal of Hydrology, 40910.1016/j.jhydrol.2011.07.041 2011.

Zhao, M., Heinsch, F.A., Nemani, R.R., & Running, S.W.: Improvements of the MODIS terrestrial gross and net primary production global data set. Remote Sensing of Environment, 95, 164-176, 10.1016/j.rse.2004.12.011, 2005.

Zhao, W.L., Gentine, P., Reichstein, M., Zhang, Y., Zhou, S., Wen, Y., Lin, C., Li, X., & Qiu, G.Y.: Physics-Constrained Machine Learning of Evapotranspiration. Geophysical Research Letters, 46, 14496-14507, 10.1029/2019gl085291, 2019.

Zheng, C., Wang, Q., & Li, P.: Coupling SEBAL with a new radiation module and MODIS products for better estimation of evapotranspiration. Hydrological Sciences Journal, 150527103244004, 10.1080/02626667.2015.1031762, 2016.